


# Antarctic erosion history reconstructed by Terre Adélie moraine geochronology

ENCELYN VOISINE<sup>1,2</sup>, YANN ROLLAND <sup>1,2</sup>, MATTHIAS BERNET<sup>2</sup>, JULIEN CARCAILLET<sup>2</sup>, GUILLAUME DUCLAUX<sup>3</sup>, JÉRÔME BASCOU<sup>4</sup>, CHRISTIAN SUE<sup>5</sup>, MÉLANIE BALVAY<sup>2</sup> and RENÉ-PIERRE MÉNOT<sup>4</sup>

<sup>1</sup>EDYTEM, Université de Savoie Mont-Blanc - CNRS, Le Bourget du Lac, France

<sup>2</sup>Université Grenoble Alpes, Université Savoie Mont-Blanc, CNRS, IRD, IFSTTAR, ISTERRE, Grenoble, France

<sup>3</sup>Université Côte d'Azur, CNRS, Géoazur, 250 rue Albert Einstein, Sophia Antipolis, France

<sup>4</sup>Université de Lyon, Université Jean Monnet, Laboratoire Magmas et Volcans, Saint-Etienne, France

<sup>5</sup>Chrono-environnement, Université de Bourgogne–Franche-Comté, Besançon, France

[yann.rolland@univ-smb.fr](mailto:yann.rolland@univ-smb.fr)

**Abstract:** We report apatite fission-track and <sup>10</sup>Be terrestrial cosmogenic nuclide (TCN) dating of 14 moraine boulders originating from inland Terre Adélie, East Antarctica. These data show cooling of the Proterozoic Terre Adélie craton at < ~120°C between 350 and 300 Ma, suggesting > 4 km temperate glacial erosion during the Late Palaeozoic Ice Age, followed by nearly null Mesozoic erosion and low glacial erosion (< 2 km) in the Cenozoic. Based on glacial flux maps, the origin of the boulders may be located ~400 km upstream. Preliminary TCN (<sup>10</sup>Be) datings of moraine boulders cluster within the last 30 ka. Cosmogenic ages from the Lacroix Nunatak suggest a main deglaciation after the Younger Dryas at *c.* 10 ka, while those of Cap Prud'homme mostly cluster at 0.6 ka, in agreement with an exhumation of boulders during the Little Ice Age.

Received 12 February 2020, accepted 17 May 2020

**Key words:** cosmogenic nuclide dating, deglaciation, exhumation, fission-track dating, Late Palaeozoic Ice Age, subglacial incision

## Introduction

Unravelling past long-term histories of glacier advances and retreats is the only way to constrain how the Antarctic ice sheet will behave in the future in a context of increasing temperatures and its impact on sea-level rise (e.g. Ritz *et al.* 2015). The East Antarctic Ice Sheet (EAIS) has the highest potential impact on eustatism, due to a combined effect of its low, mainly below sea level, continental basement elevation and its greater ice thickness (Fig. 1). However, the on-land erosional history of East Antarctica remains largely unconstrained between the Transantarctic Mountains and the Lambert Glacier (Zwartz *et al.* 1998, Verleyen *et al.* 2005, Mackintosh *et al.* 2007), and it relies largely on marine sediment analyses (e.g. Bentley *et al.* 2014). Constraining the past erosion history by means of airborne geophysical surveys (e.g. Aitken *et al.* 2016) remains speculative due to the absence of direct dating of the subglacial morphologies. Consequently, estimates of long-term (> 1 Ma) erosion of Antarctica are variable and generally ill-defined (see discussion in Rolland *et al.* 2019). On the one hand, the development of large periglacial basins during the Permian (Isbell *et al.* 2012) together with a major phase of exhumation of the Terre Adélie craton recorded at 350–300 Ma in the coastal region

(i.e. Rolland *et al.* 2019) suggest that a significant part of the glacial erosion occurred during the Late Palaeozoic Ice Age (LPIA) (Fig. 2). On the other hand, post-LPIA extensional tectonics (e.g. Lisker & Olesch 2003, Maritati *et al.* 2016, unpublished data 2019) and the largely unconstrained Cenozoic erosion (Thomson *et al.* 2013) may have also influenced the Antarctic topography and then the erosion pattern. In this context, moraines provide the opportunity to sample areas of inland East Antarctica largely hidden below the ice using thermochronology of basement rocks (e.g. Cox *et al.* 2010). Combining low-temperature thermochronology and terrestrial cosmogenic nuclide (TCN) dating of moraine boulders allows for the potential construction of the long-term erosion history of larger portions of the Antarctic continent.

Here, we report combined apatite fission-track (AFT) and <sup>10</sup>Be TCN dating of boulders from two moraines, Cap Prud'homme and Lacroix Nunatak in Terre Adélie (Fig. 1), in order to constrain the more inland erosion history of the East Antarctic basement. Based on the glacier flux maps, Cap Prud'homme is a frontal moraine located close to the Dumont D'Urville (DDU) French Base, while the Lacroix Nunatak moraine is a lateral moraine (Fig. 3). Both moraines record lithologies that are mostly different from the coastal region, including acidic volcanic rocks, sedimentary rocks and granites

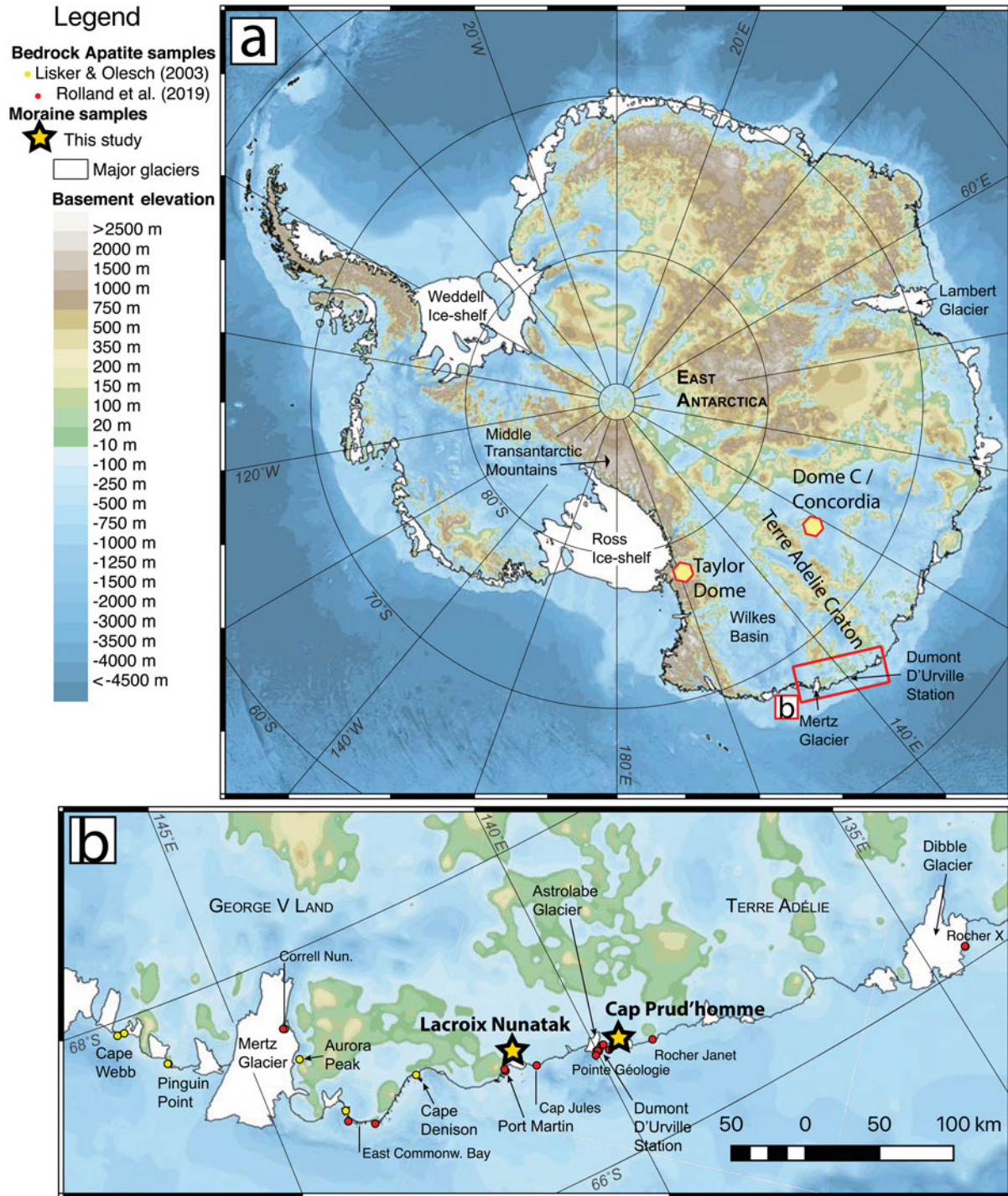


**Fig. 1.** a. General topographical map of Antarctica, with the location of Terre Adélie. b. Location of the investigated moraines and thermochronological transect in Terre Adélie-George V Land, East Antarctica. Small circles represent samples dated by apatite fission-track and apatite He dating in Lisker & Olesch (2003) (yellow circles) and Rolland *et al.* (2019) (red circles), undertaken on the Terre Adélie crystalline basement.

that do not occur along the coast (Peucat *et al.* 2002), which reflects significant transport below the ice. Although their exact source region remains unknown, the glacier flux maps suggest a probable boulder

transport of up to 500 km between 135 and 140°E as suggested by the upstream repartition of the channelized ice flow (Fig. 3) (Rignot *et al.* 2011). The AFT datings from moraines are compared to those previously

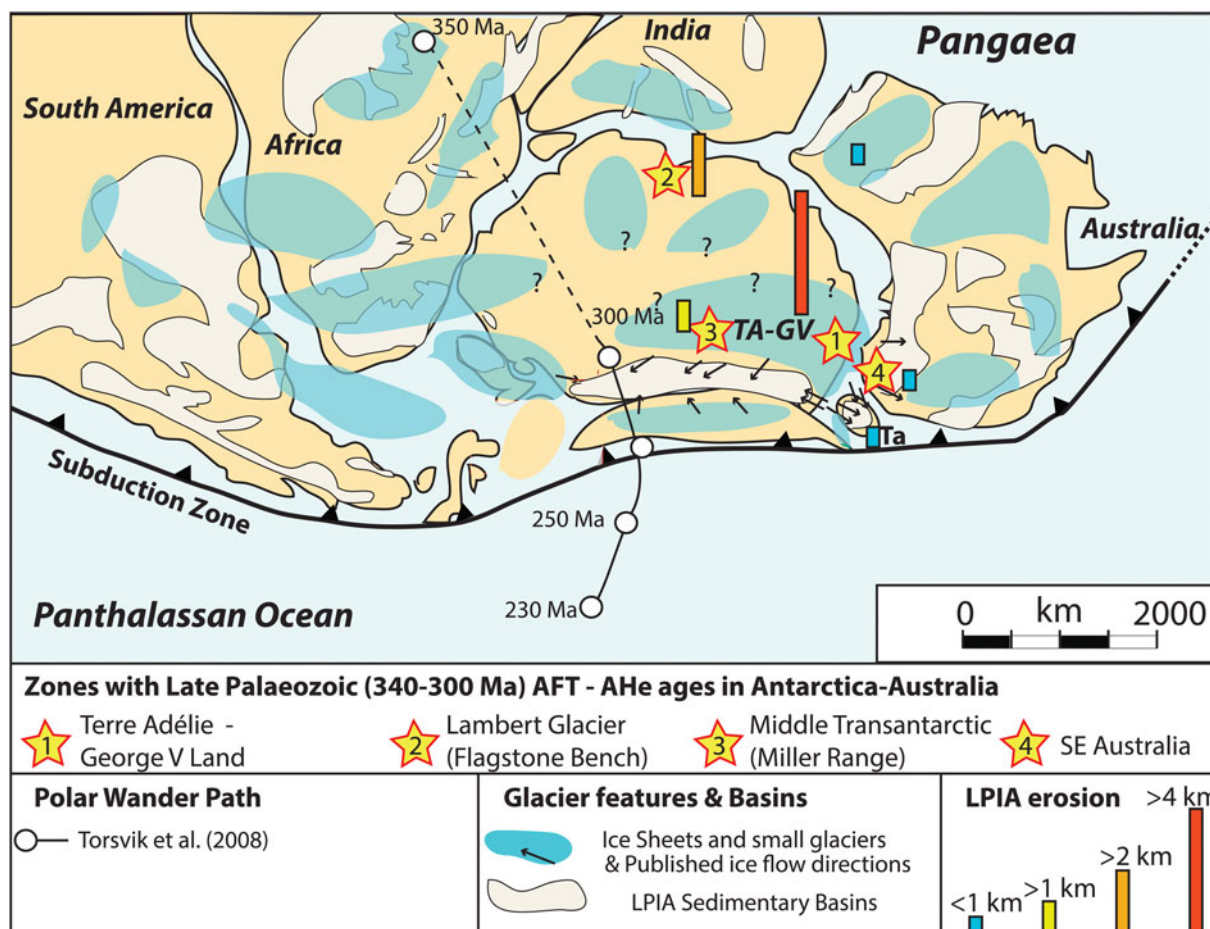


**Fig. 2.** Reconstruction of maximum glaciation during the Late Palaeozoic Ice Age (LPIA; at *c.* 300 Ma) based on glacier data compiled in Isbell *et al.* (2012) and modified from Rolland *et al.* (2019). Positions of several LPIA Antarctic ice sheets are suggested following ice-flow directions. The Terre Adélie-George V Land glacier (TA-GV) is proposed as one of the main Antarctic glaciers based on combined erosion along the Terre Adélie coast and constant ice-flow directions along the Transantarctic Mountains, while others remain speculative. The position of the South Palaeopole at 300 Ma is constrained from Torsvik *et al.* (2008). AFT = apatite fission-track, AHe = apatite helium.

obtained by Rolland *et al.* (2019) on a 600 km transect along the Terre Adélie-George V Land coast. These data are used to question the homogeneity of East Antarctica erosion towards the core of East Antarctica. The  $^{10}\text{Be}$  TCN datings are undertaken on the same boulders that have been dated by AFT to determine whether there could be any relationship between the exposure age and the source region. In addition, these datings are the first direct exposure datings undertaken on-land in Terre Adélie, and they allow us to question the age of deglaciation stages during the Quaternary.

#### Geological setting: erosion and past geological history in East Antarctica

On the basis of aerogeophysical data, the topography of the Antarctic continent is shown to be complex, which is

ascribed 1) to the erosion during early stages of glaciation (*c.* 30 Ma; Cox *et al.* 2010), 2) to efficient erosion by repeated large-scale glacier advances and retreats (e.g. Thomson *et al.* 2013, Aitken *et al.* 2016), 3) to pre-Cenozoic tectonics (e.g. Ferraccioli *et al.* 2011) and/or 4) former erosion phases inherited from the LPIA (Rolland *et al.* 2019).

In the Terre Adélie and George V Land region of East Antarctica (Fig. 1), bedrock exposures occur mainly along the coast, on small islands of  $< 1 \text{ km}^2$ . The Terre Adélie crystalline basement is made of high-grade metamorphic rocks (granulites) dating from the Neoproterozoic (*c.* 2.5 Ga) and the Palaeoproterozoic (1.6–1.7 Ga; Duclaux *et al.* 2008, Naumenko-Dèzes *et al.* 2020), accreted to a Neoproterozoic to lower Cambrian block in the eastern George V Land region (Lamarque *et al.* 2018). Almost no post-Proterozoic deformation has been recognized except for discrete east

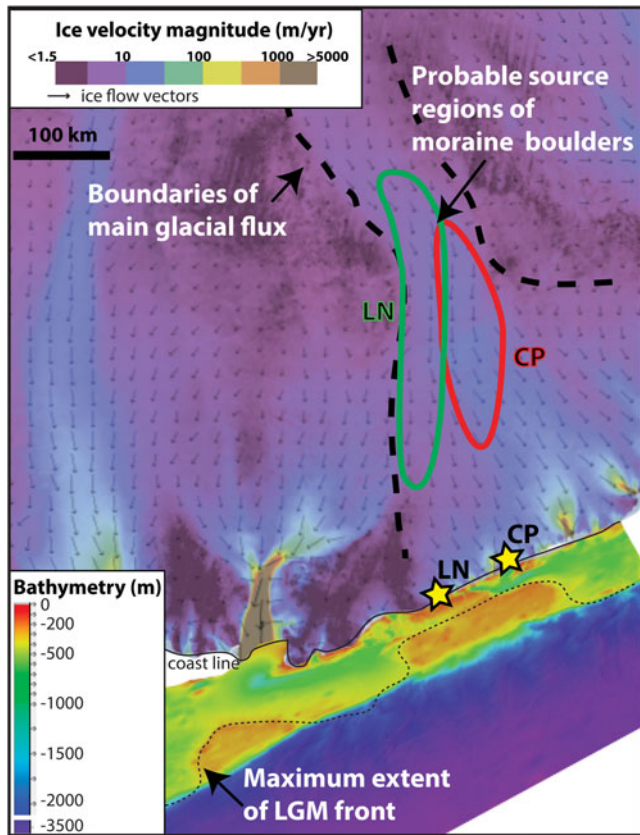


**Fig. 3.** Glacial flux map of the Terre Adélie-George V Land coast from Rignot *et al.* (2011). Note that Lacroix Nunatak (LN) is located in a lateral moraine position, while the Cap Prud'homme (CP) moraine is placed in a more frontal position with respect to the main glacial flux. The position of the Last Glacial Maximum (LGM) glacial front at 20 ka is also indicated by the dashed black line. The probable source of boulders (some 400–500 km upstream) is estimated based on the highest ice velocities in the zone of focused glacial flow. Bathymetry is from Beaman *et al.* (2011).

to west faults and joints ascribed to rifting of the Antarctic Ocean during the Mesozoic (160–95 Ma). Thermochronological data obtained across the 600 km Terre Adélie coast (Rolland *et al.* 2019) show a weighted mean of  $276 \pm 4.3$  Ma (AFT) and  $235 \pm 5.4$  Ma (apatite helium ages). Temperature-time (T-t) cooling paths based on AFT data are in agreement with a phase of cooling between 350 and 300 Ma, interpreted as glacial erosion during the LPIA (Rolland *et al.* 2019). In the neighbouring Wilkes Basin, Maritati *et al.* (unpublished data 2019) report some zircon and apatite U-Th/He age T-t modelling consistent with a slightly later erosion compatible with rifting in the Permian-Triassic (280–220 Ma). Apart from the Cenozoic ages obtained along the Transantarctic Mountains, which suggests a zone of mantle upwelling (Balestrieri *et al.* 2020), similarly old AFT ages ranging from 350 to 250 Ma were

obtained in the Miller Range of the Transantarctic Mountains, in the Lambert Glacier area (see review in Rolland *et al.* 2019). These data are in agreement with little erosion and tectonic denudation since Permian times and through Mesozoic and Cenozoic times, and thus are suggestive of mostly inefficient glacial erosion since the establishment of the polar ice sheet. In high-latitude regions, erosion is bound to be low due to the cold-based nature of glaciers, but was probably more efficient during the hottest Cenozoic interglacial periods (Thomson *et al.* 2013, Paxman *et al.* 2019). In addition, the Antarctic topography has become, on average, progressively lower-lying since 34 Ma due to ongoing subsidence below a 3 km ice cap (Paxman *et al.* 2019), which led to less efficient erosion. However, it remains the case that few data have been obtained from most of East Antarctica, which hinders any precise reconstruction of its erosion history.

### Analytical procedures

#### *Apatite fission-track geochronology*

Low-temperature thermochronology is applied to pinpoint the cooling and exhumation history of upper crustal rocks. This method permits accurate recalculating of the T-t cooling path of individual samples and reveals rapid or slow exhumation events, even in cases of long stagnation of rocks at intermediate (2–6 km) depths. We used AFT thermochronology, which is sensitive to temperatures ranging from  $\sim 60$  to  $\sim 110^\circ\text{C}$  for cooling rates of about  $4^\circ\text{C}/\text{Myr}$ , which would correspond to a hold time of  $\sim 13$  Myr within the AFT partial annealing zone (PAZ). Fission tracks are linear damage zones in the mineral lattice produced by the spontaneous fission of  $^{238}\text{U}$ , which accumulate and are preserved through time when the host mineral cools below the closure temperature, which is  $\sim 60$ – $120^\circ\text{C}$  for apatite (for details, see the references in Rolland *et al.* 2019). We measured AFT ages of collected Terre Adélie samples at the ISTERre (Université Grenoble Alpes, France) fission-track laboratory. The results are shown in Table I.

#### *Temperature-time modelling*

In case of monotonic cooling, the closure temperature can be converted into depth after estimating the palaeogeothermal gradient; the obtained cooling rate can then be translated into an exhumation rate. However, a long episode of slow cooling and/or a long hold time within the PAZ will lead to shortening of tracks at temperatures as low as  $60^\circ\text{C}$  (see references in Rolland *et al.* 2019), and thus to a younging of the apparent cooling age. In this case, the age has no

**Table I.** Apatite fission-track data.

| Sample    | <i>n</i> | $\rho_s$<br>( $10^5 \text{ cm}^{-2}$ ) | $n_s$ | $\rho_I$<br>( $10^5 \text{ cm}^{-2}$ ) | $n_i$ | $\rho_d$<br>( $10^6 \text{ cm}^{-2}$ ) | $P(\chi^2)$<br>(%) | Dispersion<br>(%) | Age<br>(Ma) <sup>a</sup> | $\pm 2\sigma$ | U<br>(ppm) | $\pm 2\sigma$ | TL<br>( <i>n</i> ) | MTL<br>( $\mu\text{m}$ ) | $\pm \sigma$ | Dpar<br>( $\mu\text{m}$ ) |
|-----------|----------|--|-------|--|-------|--|--------------------|-------------------|--------------------------|---------------|------------|---------------|--------------------|--------------------------|--------------|---------------------------|
| 16DDU-10A | 30       | 9.06                                   | 1166  | 4.84                                   | 623   | 1.40                                   | 60.8               | 0.8               | 345.9                    | 42.7          | 5          | 0             | 5                  | 12.57                    | 0.91         | 1.54                      |
| 16DDU-10E | 17       | 8.72                                   | 413   | 4.82                                   | 228   | 1.41                                   | 47.8               | 7.6               | 337.0                    | 61.2          | 5          | 1             | 2                  | 12.78                    | 0.03         | 2.08                      |
| NL 1      | 30       | 20.7                                   | 2864  | 14.3                                   | 1970  | 1.41                                   | 89.8               | 0.3               | 271.6                    | 26.5          | 15         | 1             | 7                  | 11.18                    | 1.56         | 1.20                      |
| NL 2      | 20       | 58.7                                   | 1759  | 44.5                                   | 1333  | 1.42                                   | 99.8               | 0.1               | 247.7                    | 26.3          | 47         | 3             | 32                 | 12.58                    | 1.27         | 1.60                      |
| NL 3      | 30       | 29.1                                   | 4042  | 20.5                                   | 2850  | 1.42                                   | 67.4               | 1.9               | 266.4                    | 24.8          | 22         | 1             | 43                 | 11.49                    | 2.03         | 1.42                      |
| NL 4b     | 30       | 5.88                                   | 714   | 3.95                                   | 479   | 1.42                                   | 93.0               | 0.6               | 260.5                    | 39.0          | 4          | 0             | 10                 | 11.20                    | 1.30         | 1.83                      |
| NL 5      | 25       | 15.8                                   | 1363  | 11.2                                   | 968   | 1.43                                   | 79.4               | 4.5               | 266.8                    | 30.9          | 12         | 1             | -                  | -                        | -            | 1.28                      |
| NL 6      | 8        | 28.0                                   | 487   | 23.0                                   | 400   | 1.43                                   | 99.7               | 0.0               | 231.1                    | 35.6          | 24         | 3             | -                  | -                        | -            | 1.28                      |
| NL 13     | 30       | 11.7                                   | 1927  | 6.70                                   | 1101  | 1.43                                   | 100.0              | 0.1               | 330.6                    | 35.8          | 7          | 0             | 52                 | 12.06                    | 2.38         | 1.79                      |

<sup>a</sup> Fission-track age is given as central age. Samples were analysed dry with a BX-51 Olympus microscope at 1250 $\times$  magnification. Central ages were calculated with the *Binomfit* program of M. Brandon (see Ehlers *et al.* 2005) using a  $\zeta$  value of  $283.52 \pm 14.46$ . *n* = number of grains,  $\rho_s$  = spontaneous track density,  $n_s$  = number of spontaneous tracks,  $\rho_I$  = induced track density,  $n_i$  = number of induced tracks,  $\rho_d$  = track density of the dosimeter glass (CN 5),  $P(\chi^2)$  = probability obtaining  $\chi^2$  value ( $\chi^2$  test) for *n* degrees of freedom (where *n* is the number of crystals minus 1), TL = number of measured track lengths, MTL = mean horizontal confined track length, Dpar = mean etch pit diameter of fission tracks, where each etch pit diameter was averaged from four measurements per analysed grain.

geological meaning, but the sample T-t history can be modelled based on the track-length distribution. The T-t cooling path can be used to infer the corresponding main exhumation phases and the potential phases of tectonic stagnation. Modelling of the T-t history was undertaken using *HeFTy* software based on the AFT data. The T-t *HeFTy* modelling results are displayed in Fig. 4 and Table II (for details, see the reference in Rolland *et al.* 2019).

#### Terrestrial cosmogenic nuclide <sup>10</sup>Be dating

Cosmogenic nuclide <sup>10</sup>Be dating of moraine boulders (Figs S1 & S2) was applied to highlight the most recent Cenozoic erosion and glacier history on the moraine boulders dated by AFT. Approximately 500 g of each rock sample was crushed and sieved to obtain pure quartz. The beryllium extraction was carried out at ISTerre using a protocol detailed in Darnault *et al.* (2012). The <sup>10</sup>Be measurements were obtained at ASTER, the French National Accelerator Mass Spectrometry (AMS) facility located at the Centre Européen de Recherche et d'Enseignement en Géosciences de l'Environnement (CEREGE, Aix-en-Provence), following the methods and calibrations described in Darnault *et al.* (2012). The AMS results were corrected from the process blank with <sup>10</sup>Be:<sup>9</sup>Be ratios of  $(5.4 \pm 0.7) \times 10^{15}$ . The results are shown in Table III and summarized in Table IV, and they are plotted in Fig. 5. Ages have been computed using the online CREP calculator (see Table III for details). No corrections for snow or erosion have been taken into account because of low and temporary snowfalls rapidly cleared by catabatic winds and insignificant erosion induced by permanent freezing. The sample thickness correction has been calculated with a 2.65 density factor.

## Results

### Apatite fission-track ages and T-t modelling

The moraine AFT ages obtained in this paper range from 230 to 345 Ma (Table I). We note that AFT ages of the Cap Prud'homme moraine samples are significantly older ( $335 \pm 28$  and  $345 \pm 17$  Ma) than those of Lacroix Nunatak ( $248 \pm 9$  to  $280 \pm 17$  Ma in samples NL1–6), apart from sample NL13 ( $330 \pm 12$  Ma).

The T-t modelling undertaken using fission-track lengths returned time-integrated T-t paths with a significant cooling in the Late Palaeozoic from  $> 150^\circ\text{C}$  to  $\sim 50^\circ\text{C}$ , in the range 350–300 Ma (Table II). Exhumation rates  $> 0.25 \text{ mm yr}^{-1}$  are estimated for the 340–300 Ma time range, based on a standard continental geotherm in agreement with the cratonic nature of Terre Adélie. After this abrupt exhumation, which terminated at *c.* 300 Ma, the samples followed a more or less quiescent Mesozoic history. The T-t paths followed a slow exhumation  $< 0.005 \text{ mm yr}^{-1}$  pattern during the Mesozoic until 40–30 Ma (Fig. 4). Regarding this very long stay at depths close to the apatite PAZ, the AFT ages should not be taken as geologically meaningful ages, and only the T-t models should be considered as representative of their thermal history. Finally, a small acceleration of cooling occurred since 40–30 Ma, which represents 1–2 km of exhumation in most samples.

### Cosmogenic nuclide dating

The TCN <sup>10</sup>Be ages obtained in the two moraines range from 31.8 to 0.47 ka and fall within five age groups (Fig. 5 & Table III), mostly spread after the Last Glacial Maximum (LGM): 1) a first age group at  $\sim 32$  ka is represented by two samples, one sample from each

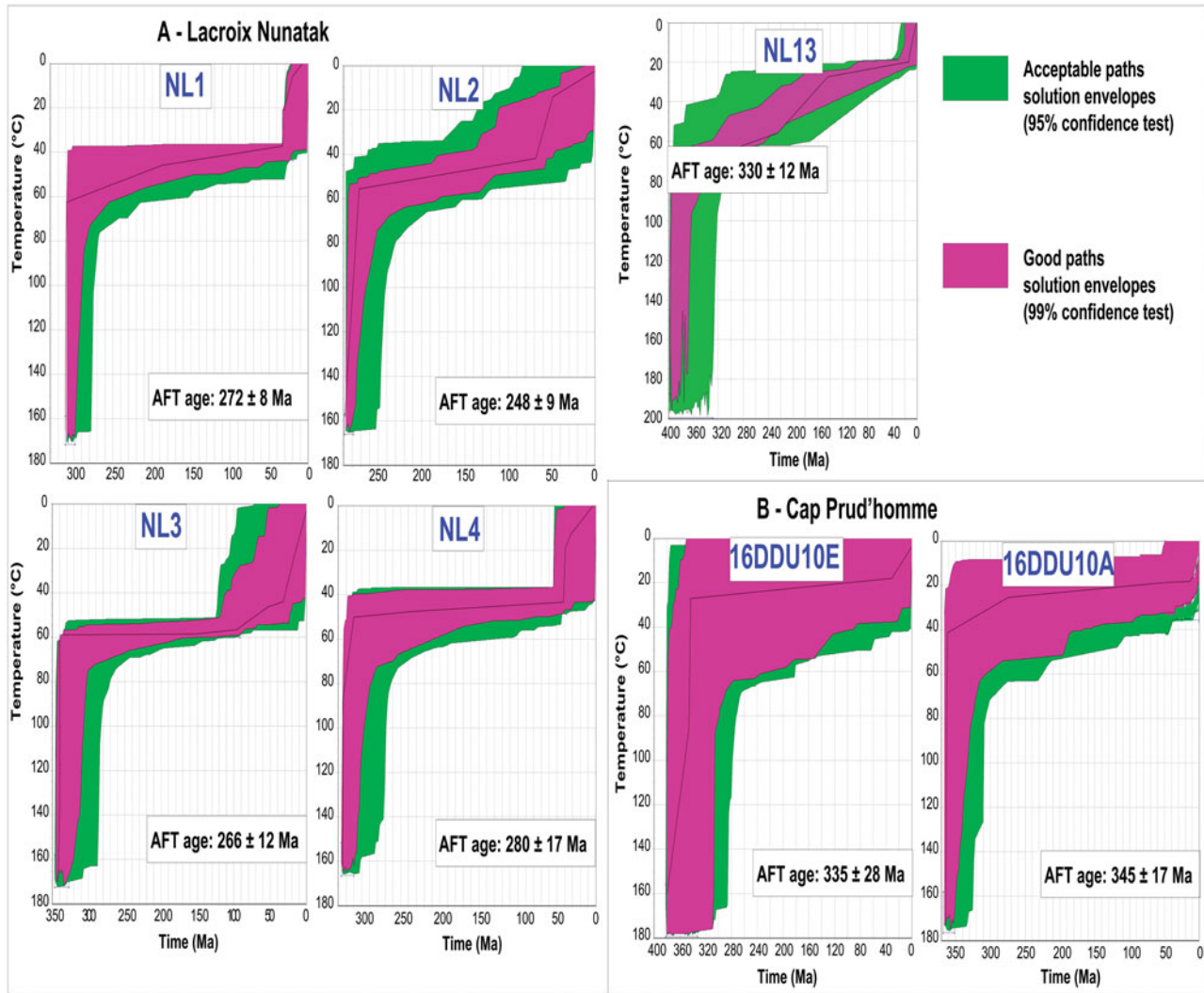


**Fig. 4.** Time-temperature paths of individual samples using *HeFTy* modelling results. The modelling is based on the apatite fission-track (AFT) data (Tables I & II).

moraine. The other TCN datings are post-LGM: 2) the oldest post-LGM age is of  $14.7 \pm 1.4$  ka at Lacroix Nunatak. Following this age, three distinct Holocene age peaks are dated and at 3)  $9.4\text{--}10.4$  ka ( $n = 2$ ), 4)  $3.0 \pm 0.2$  ka ( $n = 4$ ) and 5)  $570 \pm 48$  yr ( $n = 3$ ), respectively.

**Discussion**

*Insights for the Late Palaeozoic to Mesozoic erosion history*

As previously noted for basement samples dated by AFT along the Terre Adélie coast, the modelled T-t paths record a large amount of exhumation during Carboniferous times (Figs 4 & 6). The exhumation paths for the source regions of the two moraine samples are broadly similar to those of the Terre Adélie coast. Thus, this age span is slightly older than that of Permian rifting (e.g. Lisker & Olesch 2003), and is more in

agreement with that of the LPIA (e.g. Isbell *et al.* 2012). The LPIA started in the Late Devonian and extended until the early Late Permian (360–260 Ma), which represents the longest and most prominent glacial event in Earth's history (e.g. Qie *et al.* 2019). This glacial phase is ascribed to atmospheric CO<sub>2</sub> drawdown or increased volcanism (Montañez *et al.* 2016). A sea-level drawdown of approximately -30 to -70 m is documented since 340 Ma, and peaked at 310–290 Ma (Rygel *et al.* 2008), which supports the hypothesis of an extensive polar ice sheet in this time range. The LPIA culminated during the Late Carboniferous, at 330–300 Ma, in the Southern Hemisphere (e.g. Isbell *et al.* 2012), when the South Pole was close to its present position (Fig. 2) (see discussions in Isbell *et al.* 2012). The similar AFT ages and cooling at 330–300 Ma obtained along the Terre Adélie coast and in the moraine boulders suggest a

**Table II.** Summary of *HeFTy* modelling results based on apatite fission-track (AFT) data.

| Sample   | Accepted paths | Good paths | AFT (Ma)    | GOF  | MTL ( $\mu\text{m}$ ) | Model MTL ( $\mu\text{m}$ ) |
|----------|----------------|------------|-------------|------|-----------------------|-----------------------------|
| 16DDU10A | 404            | 284        | 346 +47/-14 | 1.00 | 14.2 $\pm$ 0.6        | 14.7 $\pm$ 0.6              |
| 16DDU10E | 756            | 1079       | 336 +66/-56 | 0.99 | 14.4 $\pm$ 0.7        | 14.8 $\pm$ 0.7              |
| NL1      | 244            | 139        | 272 +29/-26 | 1.00 | 13.2 $\pm$ 0.9        | 14.0 $\pm$ 0.9              |
| NL2      | 306            | 60         | 248 +29/-26 | 0.99 | 14.1 $\pm$ 0.9        | 14.2 $\pm$ 1.0              |
| NL3      | 376            | 112        | 266 +27/-24 | 1.00 | 11.5 $\pm$ 2.1        | 11.6 $\pm$ 2.0              |
| NL4B     | 428            | 274        | 280 +43/-37 | 1.00 | 13.3 $\pm$ 0.9        | 13.9 $\pm$ 0.9              |
| NL13     | 1212           | 270        | 331 +39/-35 | 0.99 | 13.9 $\pm$ 1.3        | 14.3 $\pm$ 1.1              |

Results are based on 10 000 model runs. The MTL values are given as *c*-axis projected track lengths. The AFT ages calculated by *HeFTy* are pooled ages. Initial track lengths are estimated from mean etch pit diameters of fission tracks with 5.5 M HNO<sub>3</sub>. The GOF refers to the modelling quality value ranked between 0 and 1.

GOF = goodness of fit, MTL = mean horizontal confined track length.

major erosion phase during the LPIA at the scale of East Antarctica (Fig. 3). Thermochronological studies undertaken around East Antarctica reveal similar cooling paths and ages (Arne 1994, Fitzgerald 1994, Lisker & Olesch 2003). Taken together, these data are suggestive of a large ice cap that covered the whole East Antarctic continent in the Late Carboniferous. This is also supported by the erosion and transport of sediments in radial directions towards large peripheral glacial basins during the Permo-Carboniferous (Isbell *et al.* 2012, Rolland *et al.* 2019).

#### Regional-scale Cenozoic erosion

Several aspects of the modelled T-t paths can be attributed to Cenozoic tectonics. The two Cap Prud'homme samples (16DDU10A and 10E) rapidly cooled to 20–30°C at *c.* 340 Ma, whereas the Lacroix Nunatak samples rapidly cooled to 50–60°C at between 350 and 300 Ma (Fig. 4). This difference is ascribed to a smaller Cenozoic erosion (< 1 km) in the source region of the dated Cap Prud'homme moraine samples than in that of the dated Lacroix Nunatak boulders (> 1.5–2.0 km) and of the Terre Adélie coast. Based on the current glacier flux maps (Fig. 3) (Rignot *et al.* 2011), Cap Prud'homme appears to be positioned in a more frontal moraine position, whereas the Lacroix Nunatak moraine appears to be on the side of the glacial flux, positioned as a lateral moraine on the margins of some highlands (Fig. 3). During the Early Cenozoic, the significantly thinner ice sheet would preferentially drain through adjacent lowlands rather than the relatively highly elevated Terre Adélie craton (see Cox *et al.* 2010 for a similar discussion of other subglacial highlands in East Antarctica). Thus, one possible explanation would be that the Cap Prud'homme boulders are sourced from a higher-elevated area within the craton that may have been protected from high levels of erosion due to the presence of ice caps during the Cenozoic.

The glacier flux map suggests that moraine samples might have originated from a focused erosion loci

located upstream of the Terre Adélie glacial flux (Fig. 3). Such narrow zones of focused channelized flow have been confirmed in the whole Antarctic ice sheet (e.g. Morlighem *et al.* 2019). These narrow corridors could have been incised during the Mid-Pliocene warm period (e.g. Paxman *et al.* 2019). These latter authors inferred a dynamic erosional environment based on the development of plateau features on the neighbouring Wilkes Subglacial Basin at *c.* 3.5 Ma. More samples would be necessary to test this hypothesis in Terre Adélie.

#### Cosmogenic nuclide dating of moraines reveals post-LGM glacier dynamics

The significance of the diverse TCN <sup>10</sup>Be ages obtained in the two moraines, ranging from 31.8 to 0.47 ka (Fig. 4 & Table I), is still uncertain, as they might result from either distinct deglacial events or a combination of inheritance and a progressive Holocene deglacial process. Each moraine has to be considered separately to make a reasonable interpretation of this first batch of terrestrial cosmogenic ages (e.g. D'Arcy *et al.* 2019, Žebre *et al.* 2019). Based on the most probable hypothesis that a moraine formed in a single deglacial stage (e.g. Putkonen & Swanson 2003, Heyman *et al.* 2011), we propose the following interpretation of our dataset:

- The Lacroix Nunatak moraine shows three ages spread between the Late Glacial to Early Holocene (14.7, 10.3 and 9.4 ka), which suggests a main deglaciation stage directly following the Younger Dryas cold event as elsewhere in Antarctica (e.g. Çiner *et al.* 2019). Subsequently, it is most probable that the 29.5 ka age represents some inheritance from a previous deglacial stage, and is thus considered as not geologically meaningful and a minimum age for this previous event. By the same logic, the remaining boulders with ages ranging from 4.4 to 2.1 ka are considered as outliers, which may reflect a late exhumation process of these boulders. The fact that they show a relatively close cluster of values could be ascribed to a phase of

**Table III.** Terrestrial cosmogenic nuclide results of the Lacroix Nunatak (samples quoted as NL) and Cap Prud'homme moraines (samples quoted as 16DDU).

| Sample   | Latitude (°S) | Longitude (°E) | Elevation (m a.s.l.) | Sample information | Thickness (cm) | Shielding factor | Scaled production rate                    |             | <sup>10</sup> Be concentration <sup>a</sup>                    |             | Ages <sup>b,c</sup> |                      |                      |
|----------|---------------|----------------|----------------------|--------------------|----------------|------------------|---|-------------|--|-------------|---------------------|----------------------|----------------------|
|          |               |                |                      |                    |                |                  | Value                                     | Uncertainty | Value  | Uncertainty | Value               | External uncertainty | Internal uncertainty |
|          |               |                |                      |                    |                |                  | (atoms g <sup>-1</sup> yr <sup>-1</sup> ) |             | (×10 <sup>3</sup> atoms g Qtz <sup>-1</sup> yr <sup>-1</sup> ) |             | (ka)                |                      |                      |
| 16DDU10A | 66°41'20.12"  | 139°54'18.64"  | 20                   | Orthogneiss        | 2.0            | 1                | 5.07                                      | 0.24        | 157.36   | 8.15        | 31.71               | 2.18                 | 1.64                 |
| 16DDU10B | 66°41'19.96"  | 139°54'18.63"  | 12                   | Gneiss             | 3.0            | 1                | 5.07                                      | 0.24        | 20.98  | 3.16        | 4.23                | 0.67                 | 0.64                 |
| 16DDU10D | 66°41'19.62"  | 139°54'18.41"  | 15                   | Red sandstone      | 3.0            | 1                | 5.07                                      | 0.24        | 2.32   | 0.31        | 0.47                | 0.07                 | 0.06                 |
| 16DDU10E | 66°41'20.05"  | 139°54'18.52"  | 12                   | Red sandstone      | 4.5            | 1                | 5.07                                      | 0.24        | 3.47   | 0.44        | 0.71                | 0.10                 | 0.09                 |
| 16DDU10G | 66°41'19.43"  | 139°54'18.53"  | 10                   | Red sandstone      | 4.0            | 1                | 5.07                                      | 0.24        | 2.99   | 0.42        | 0.61                | 0.09                 | 0.09                 |
| NL1      | 66°50'50.83"  | 141°21'21.25"  | 51                   | Leucogranite       | 2.0            | 1                | 5.52                                      | 0.26        | 24.09  | 2.49        | 4.44                | 0.50                 | 0.46                 |
| NL2      | 66°50'54.39"  | 141°21'22.45"  | 60                   | Migmatite          | 3.0            | 1                | 5.52                                      | 0.26        | 55.67  | 8.18        | 10.33               | 1.58                 | 1.51                 |
| NL3      | 66°50'49.87"  | 141°21'21.01"  | 55                   | Migmatite          | 3.0            | 1                | 5.52                                      | 0.26        | 15.33  | 2.00        | 2.84                | 0.39                 | 0.37                 |
| NL4A     | 66°50'20.61"  | 141°21'22.05"  | 65                   | Granodiorite       | 2.0            | 1                | 5.52                                      | 0.26        | 11.37  | 1.82        | 2.09                | 0.34                 | 0.33                 |
| NL9      | 66°50'50.83"  | 141°21'45.36"  | 70                   | Migmatite          | 3.0            | 1                | 5.52                                      | 0.26        | 158.10   | 11.22       | 29.49               | 2.48                 | 2.09                 |
| NL10     | 66°51'01.03"  | 141°21'53.42"  | 75                   | Gneiss             | 1.0            | 1                | 5.52                                      | 0.26        | 80.20  | 6.58        | 14.65               | 1.37                 | 1.20                 |
| NL13     | 66°50'50.83"  | 141°21'21.32"  | 63                   | Granite            | 5.0            | 1                | 5.52                                      | 0.26        | 49.72  | 6.97        | 9.38                | 1.38                 | 1.31                 |

<sup>a</sup> Accelerator mass spectrometry (AMS) analyses have been carried out at the French AMS facility ASTER. The <sup>10</sup>B concentrations were calibrated against the in-house Centre Européen de Recherche et d'Enseignement en Géosciences de l'Environnement (CEREGE) standard using the theoretical <sup>10</sup>Be:<sup>9</sup>Be ratio of 1.191 × 10<sup>-11</sup> and a <sup>10</sup>Be half-life of 1.387 ± 0.012 10<sup>6</sup> years (Chmeleff *et al.* 2010, Korschinek *et al.* 2010). Results have been corrected from the chemical blank (<sup>10</sup>Be:<sup>9</sup>Be<sub>blank</sub> = 5.39 ± 0.67 × 10<sup>-15</sup>). Propagated uncertainties include counting statistics, a conservative estimate of 0.5% for instrumental variability and the uncertainty of the standard deviation and chemical blank.

<sup>b</sup> Ages have been computed with the online CREP calculator using a worldwide production rate of 4.09 ± 0.19 at g<sup>-1</sup> yr<sup>-1</sup>, the time-dependent scaling scheme Lal/Stone with ERA-40 and the geomagnetic record of Lifton (2016).

<sup>c</sup> Internal uncertainties consider the analytical uncertainties, while the external uncertainties include ~4.5% uncertainty in the production rate and 8% uncertainty in the <sup>10</sup>Be decay constant. The sample thickness correction has been calculated with a 2.65 density factor.

a.s.l. = above sea level.



**Table IV.** Summary of apatite fission-track (AFT) and cosmogenic nuclide dating results.

| Sample        | NL1   | NL2   | NL3   | NL4   | NL5   | NL6   | NL9   | NL10  | NL13  | 16DDU10A | 16DDU10B | 16DDU10D | 16DDU10E | 16DDU10G |
|---------------|-------|-------|-------|-------|-------|-------|-------|-------|-------|----------|----------|----------|----------|----------|
| AFT           | 271.6 | 247.6 | 266.4 | 280.2 | 265.7 | 230.8 | -     | -     | 330.4 | 345.7    | -        | -        | 335.1    | -        |
| $\pm 1\sigma$ | 8     | 9     | 12    | 17    | 11    | 16    | -     | -     | 12    | 17       | -        | -        | 28       | -        |
| Cosmogenic    | 4.43  | 10.33 | 2.84  | 2.09  | -     | -     | 29.49 | 14.65 | 9.38  | 31.71    | 4.23     | 0.47     | 0.71     | 0.61     |
| $\pm 1\sigma$ | 0.50  | 1.58  | 0.39  | 0.34  | -     | -     | 2.49  | 1.37  | 1.38  | 2.20     | 0.67     | 0.07     | 0.1      | 0.09     |

Undated samples are due to the absence or insufficient number of apatite (AFT) and quartz for  $^{10}\text{Be}$  dating.

increased ice depletion of the moraine related to a climatic cause.

- The Cap Prud'homme moraine shows a repartition of block ages that appears to be more random. Again, one age of 31.2 ka could be ascribed to inheritance as in Lacroix Nunatak. The other ages are much younger, with one of mid-Holocene age (4.2 ka) and all the rest being very young (0.5–0.7 ka). Therefore, one tentative interpretation could be that the main exhumation event is very recent one (*c.* 0.6 ka) for this moraine, and that the 4.2 and 31.2 ka ages represent some inheritance for the two blocks. Despite the fact that samples are just > 10 m above sea level, it is improbable that they could have been below sea level several ka ago, as a null vertical motion is measured by GPS in this area (Li *et al.* 2020). Therefore, the young exhumation age of *c.* 0.6 ka could be ascribed to a complex exhumation dynamic of boulders in an ice matrix as reflected by the works of Tison *et al.* (1993) and Genthon *et al.* (2007).

In conclusion, two main deglacial ages can be proposed from the two moraines: a significant early Holocene deglacial age at Lacroix Nunatak, most probably during the Younger Dryas (*c.* 11 ka) and a very young deglaciation age (*c.* 0.6 ka) in Cap Prud'Homme. Based on other evidence from offshore sediment cores and inland ice dynamics, we propose below a summary of possible evolution of the Terre Adélie coast since the LGM.

- 1) Based on the bathymetry maps compiled by Beaman *et al.* (2011) and on the offshore sediment analysis of Domack *et al.* (1989) and Crosta *et al.* (2007), the palaeoglacier flow and maximum extent during the LGM are identified offshore of the Terre Adélie coast, where it reached at least the rim of the continental plateau (Figs 3 & 7c). This frontal LGM moraine thus stands at 80–130 km north of the current shoreline (Bentley *et al.* 2014). The orientation of basins suggests a dominant north-west-directed and episodic north-directed glacial flux during the LGM (Fig. 7).
- 2) Based on the age of the Lacroix Nunatak moraine, the oldest post-LGM age is  $14.7 \pm 1.4$  ka at Lacroix Nunatak. However, with only one age, this sample could still reflect some partial inheritance and still needs confirmation. This age is similar to the main deglaciation age of meltwater pulse 1A ('MWP-1A'), which coincides with an abrupt deglacial warming recorded at Taylor Dome at  $\sim 14.6$  ka (Fig. 7a) (Steig *et al.* 2000) at the latitude of the potential glacial sources of the Terre Adélie glaciers. Similar ages are recorded by Balco *et al.* (2019) in neighbouring Victoria Land and correlate with a rapid eustatic sea-level rise and deglaciation at higher latitudes. This

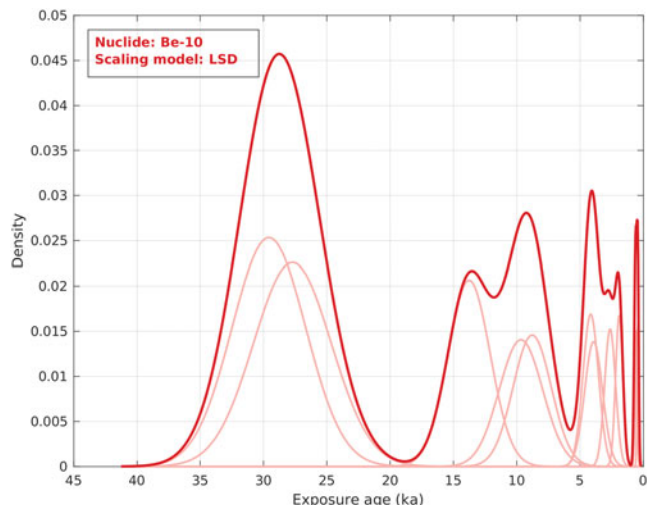


**Fig. 5.** Probability density distribution of <sup>10</sup>Be cosmogenic ages as a function of the exposure age (see Table III for details). Five age peaks are distinguished at ~30 ka, ~14.7 ka, ~10 ka, ~3 ka and ~570 yr. LSD = Lifton-Sato-Dunai scaling.

is expressed both at South Hemisphere mid-latitudes and at North Hemisphere mid- to high latitudes, such as in the Alps (e.g. Darnault *et al.* 2012).

Following this age, three distinct Holocene-age peaks are dated as follows:

- 3) The first group is dated at 9.4–10.4 ka. These two Early Holocene ages at  $9.4 \pm 1.4$  ka and  $10.4 \pm 1.6$  ka correspond to the age of the Lacroix Nunatak moraine and may correspond to the deglaciation stage directly following the Younger Dryas cold event (e.g. Çiner *et al.* 2019). This 10–11 ka age corresponds to the onset of an increased glacial flux, with rates  $> 4$  cm ice yr<sup>-1</sup> recorded at the Taylor Dome ice core (Fig. 7a) (Steig *et al.* 2000). This reflects a change in climate dynamics for the EAIS, as also suggested by the marine records off the Terre Adélie coast (Bentley *et al.* 2014). This climatic phase is well expressed at the scale of the Antarctic continent (e.g. Çiner *et al.* 2019), and is also largely documented at mid-latitudes (e.g. Darnault *et al.* 2012).
- 4) The second group of Holocene ages is recorded in four samples from the two moraines, spanning between  $4.4 \pm 0.5$  and  $2.1 \pm 0.3$  ka. This age range correlates with a phase of deglaciation that closely follows a stage of glacier re-advance at *c.* 5 ka (Steig *et al.* 2000), most probably due to increased precipitation during the Holocene climate optimum. We propose that this climatic event might have led to the exhumation of moraine blocks.
- 5) Finally, the last Holocene age peak of  $570 \pm 48$  yr is represented by three ages of the Cap Prud'homme

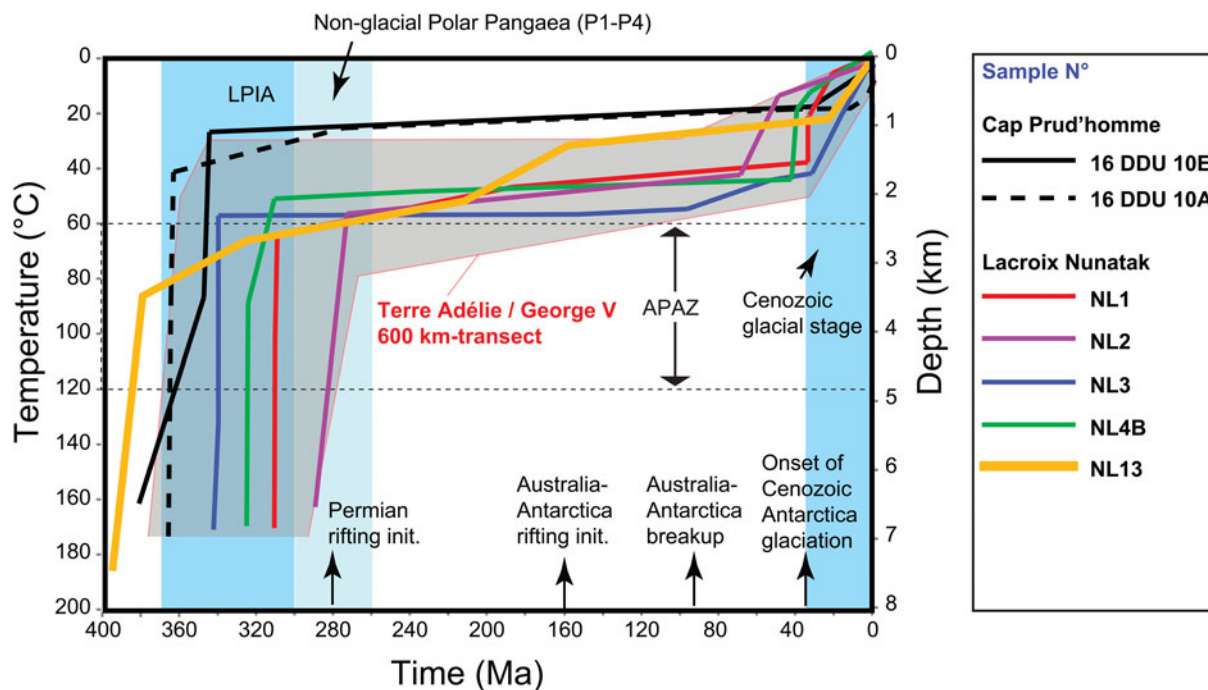


**Fig. 6.** Summary of time-temperature results using *HeFTy* modelling, with main tectonic events and glaciations of the Phanerozoic (Isbell *et al.* 2012 and references therein). The depth in kilometres or equivalent amount of exhumation is estimated based on a thermal gradient of 25°C km<sup>-1</sup>, in agreement with the crustal thickness of the Terre Adélie craton (Lamarque *et al.* 2015). APAZ = apatite partial annealing zone of fission tracks, LPIA = Late Palaeozoic Ice Age, P1–P4 = glaciation events occurring in Australia in the Permian (300–260 Ma).

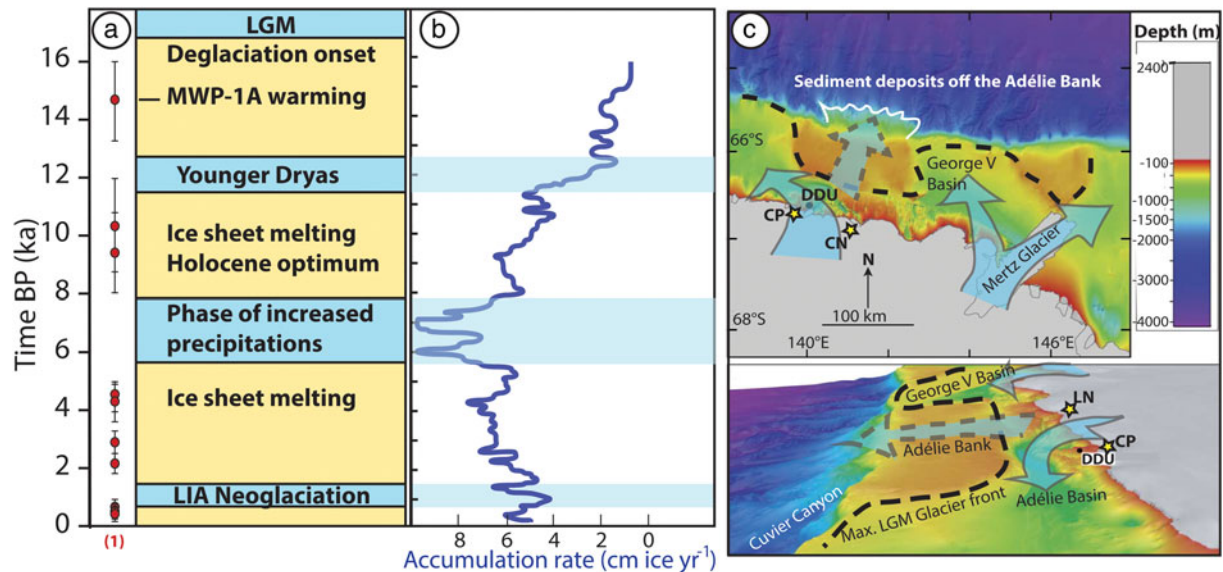


**Fig. 7.** **a.** The <sup>10</sup>Be cosmogenic nuclide dating results (this paper) and post-Last Glacial Maximum (LGM) climatic model reconstructed for the Terre Adélie-George V Land domain from Steig *et al.* (2000). **b.** Variations of ice accumulation rate at the Taylor Dome since 16 ka (Steig *et al.* 2000). **c.** George V digital elevation model bathymetric map of the Terre Adélie-George V Land coast and perspective view (towards the east) of the Terre Adélie coast, showing the prominence of the Adélie Bank, modified after Beaman *et al.* (2011). The locations of the investigated moraines are indicated by yellow stars (CP = Cap Prud'homme, LN = Lacroix Nunatak). The direction of flow of glaciers during the LGM is indicated by the blue arrows and the frontal glacier grounding line during the LGM is shown by the bold dashed lines. The major glacial pathway for the Dumont D'Urville (DDU) area is towards the north-west along the Adélie Basin. Sediment deposits off the Adélie Bank suggest episodic glacial transport towards the north over the Adélie Bank during the LGM. LIA = Little Ice Age.

moraine ranging between  $470 \pm 70$  and  $710 \pm 100$  yr. These ages are within the Little Ice Age (LIA) range, which is defined from  $\sim 1300$  to 1850 yr CE. These latter ages are most probably ascribed to very recent deglaciation of boulders given the field situation (Fig. S1), with some inherited component. It might also reflect an accelerated retreat of the glacier tongue since the end of the LIA, which is in agreement with the observations of DDU in 1840, who described a glacier front at  $\sim 20$  km north of its present position (Godard *et al.* 2017).

#### *Considerations regarding the obtained <sup>10</sup>Be ages from the perspective of future works*

Most of the East Antarctic basement stands at elevations of  $< 0$  m between 100 and 160°E (Fig. 1). This portion of the continent is potentially the most sensitive to sea-level fluctuations induced by the response of the EAIS to rising sea temperature, which is a central parameter in controlling the evolution of the ice cap. In this context, palaeoproxy records and long-term observational datasets are underused resources in terms of strategies for improving Antarctic climate projections for the twenty-first century and beyond (Bracegirdle *et al.* 2019). Documenting the response of the EAIS to the environmental conditions that led to the deglaciation

after the LGM will provide a basis for understanding and modelling its future response to climate warming over the coming centuries. The ice sheet was generally more extensive than was present during the global LGM (27–20 ka BP; Clark *et al.* 2009). Based on the sparse and mostly marine records along the East Antarctic coast, previous studies suggested that the EAIS responded with a delay of *c.* 6–8 ka to the increasing temperatures after the LGM (Bentley *et al.* 2014). As suggested by marine records, the EAIS response to deglaciation may have followed a three-stage model (Bentley *et al.* 2014):

- 1) Onset of ice sheet retreat as early as 18 ka BP in the Lambert/Amery system, perhaps due to an enhanced sensitivity related to a rapid post-glacial sea-level rise at that time (Golledge *et al.* 2012).
- 2) Retreat at some sites at 14 ka BP, coinciding with MWP-1a, during which the global sea level rose by between 16 and 25 m in  $\sim 400$ –500 years. However, Bentley *et al.* (2014) see a small contribution of the Antarctic to the sea-level rise during MWP-1A.
- 3) The majority of ice-sheet retreat occurred at the onset of the Holocene (12 ka BP) in response to oceanic warming (Bentley *et al.* 2014) and coinciding with the Early Holocene warm period recorded in coastal ice cores and lake sediment records (Verleyen *et al.*

2011). This seems to be in disagreement with the inner EAIS glacial record of Taylor Dome (Fig. 7a) (Steig *et al.* 2000), which may indicate that the EAIS responded more rapidly to MWP-1A than is suggested by the marine records. However, in accordance with the marine records, it seems that the Holocene deglacial signal is the most expressed from our  $^{10}\text{Be}$  TCN age dataset. Erosion of some of the former glacial remains during the Younger Dryas re-advance may also have hidden part of the moraine record.

Therefore, a more precise establishment of the EAIS behaviour in relation to climate change since the LGM requires further testing through measurement of past glacial extensions onshore of East Antarctica, especially in Terre Adélie. Our preliminary dataset shows that the  $^{10}\text{Be}$  dating technique is appropriate for this goal. The combined use of thermochronology on the same boulders may allow us to infer the domains preferentially eroded during each of the climatic phases, which may be used as a proxy of subglacial erosion dynamics over the long term, but this requires a large number of dated samples and a detailed geomorphological analysis of moraines.

## Conclusion

Combined thermochronology and cosmogenic nuclide analysis of moraine blocks is shown to be a powerful tool for investigating both the past (Phanerozoic) and recent (Cenozoic-Quaternary) erosion history of hidden Antarctica. The AFT dating of moraine blocks in Terre Adélie seems to be in agreement with a major phase of (hot-based) glacial erosion during the LPIA between 350 and 300 Ma and a null erosion-exhumation during the Mesozoic. Furthermore, a moderate and focused local Cenozoic erosion (< 1.5–2.0 km) is recorded in samples both several hundreds of kilometres upstream and along the coast of the Terre Adélie craton, which is ascribed to a low level of erosion of the East Antarctic margin since the establishment of the polar ice sheet. This low level of erosion is possibly due to the omnipresence of cold-based glaciers since 34 Ma. The geometry of the glacial flux is suggestive of the development of over-deepening in narrow corridors in relation to the mid-Pliocene warm period some 400–500 km upstream of the investigated moraines. The  $^{10}\text{Be}$  cosmogenic nuclide surface exposure ages of the moraine boulders indicate a major deglaciation after the Younger Dryas, which might have commenced at *c.* 14.7 ka and become significantly amplified after 10 ka. The timing of retreats is found to be similar to phases observed in the Northern Hemisphere and at mid- to high latitudes.

## Acknowledgements

We warmly thank F. Coeur and F. Senebier (GeoThermoChronology Platform, ISTERre) for mineral separation support and K. Kedadouche and G. Aumaitre for TCN analysis. C. Ritz and P. Valla are thanked for discussions. In addition, this manuscript was significantly enhanced following the constructive comments of A. Çiner and an anonymous reviewer.

## Author contributions

YR conceived the study and wrote the paper. EV took part in the AFT and cosmogenic nuclide dating analyses during his Master's internship. MB supervised the AFT datings, prepared the samples and checked all of the results. JC supervised the cosmogenic datings. JB and CS assisted in field sampling. R-PM and GD provided support regarding the artwork and expertise in Antarctic geology.

## Financial support

This work was supported by a LABEX grant from Université Grenoble Alpes and ISTERre. The Institut Paul-Émile Victor supported numerous field seasons in Terre Adélie through the Géologie du Craton de Terre Adélie (GEOLETA) and Architecture de la Lithosphère de la Terre Adélie (ARLITA) programmes.

## Details of data deposit

The data can be retrieved at <https://hal.archives-ouvertes.fr>.

## Supplemental material

Two supplemental figures will be found at <https://doi.org/10.1017/S095410202000036X>.

## References

- AITKEN, A.R.A., ROBERTS, J.L., VAN OMMEN, T.D., YOUNG, D.A., GOLLEGE, N.R., GREENBAUM, J.S., *et al.* 2016. Repeated large-scale retreat and advance of Totten Glacier indicated by inland bed erosion. *Nature*, **533**, 385–389.
- ARNE, D.C. 1994. Phanerozoic exhumation history of northern Prince Charles Mountains (East Antarctica). *Antarctic Science*, **6**, 69–84.
- BALCO, G., TODD, C., GOEHRING, B.M., MOENING-SWANSON, I. & NICHOLS, K. 2019. Glacial geology and cosmogenic-nuclide exposure ages from the Tucker Glacier-Whitehall Glacier confluence, northern Victoria Land, Antarctica. *American Journal of Science*, **319**, 255–286.
- BALESTRIERI, M.L., OLIVETTI, V., ROSSETTI, F., GAUTHERON, C., CATTÒ, S. & ZATTIN, M. 2020. Topography, structural and exhumation history of the Admiralty Mountains region, northern Victoria Land, Antarctica. *Geoscience Frontiers*, 10.1016/j.gsf.2020.01.018.
- BEAMAN, R.J., O'BRIEN, P.E., POST, A.L. & DE SANTIS, L. 2011. A new high-resolution bathymetry model for the Terre Adélie and George V continental margin, East Antarctica. *Antarctic Science*, **23**, 95–103.
- BENTLEY, M.J., COFAIGH, C.O., ANDERSON, J.B., CONWAY, H., DAVIES, B., GRAHAM, A.G., *et al.* 2014. A community-based geological

- reconstruction of Antarctic ice sheet deglaciation since the Last Glacial Maximum. *Quaternary Science Reviews*, **100**, 1–9.
- BRACEGIRDLE, T.J., COLLEONI, F., ABRAM, N.J., BERTLER, N.A., DIXON, D.A., ENGLAND, M., *et al.* 2019. Back to the future: using long-term observational and paleo-proxy reconstructions to improve model projections of Antarctic climate. *Geosciences*, **9**, 255.
- CHMELEFF, J., VON BLANCKENBURG, F., KOSSERT, K. & JAKOB, D. 2010. Determination of the  $^{10}\text{Be}$  half-life by multicollector ICP-MS and liquid scintillation counting. *Nuclear Instruments and Methods in Physics Research Section B: Beam Interactions with Materials and Atoms*, **268**, 192–199.
- ÇINER, A., YILDIRIM, C., SARIKAYA, M.A., SEONG, Y.B. & YU, B.Y. 2019. Cosmogenic  $^{10}\text{Be}$  exposure dating of glacial erratics on Horseshoe Island in western Antarctic Peninsula confirms rapid deglaciation in the Early Holocene. *Antarctic Science*, **31**, 319–331.
- CLARK, P.U., DYKE, A.S., SHAKUN, J.D., CARLSON, A.E., CLARK, J., WOHLFARTH, B., *et al.* 2009. The Last Glacial Maximum. *Science*, **325**, 710–714.
- COX, S.E., THOMSON, S.N., REINERS, P.W., HEMMING, S.R. & VAN DE FLIERDT, T. 2010. Extremely low long-term erosion rates around the Gamburtsev Mountains in interior East Antarctica. *Geophysical Research Letters*, **37**, L22307.
- CROSTA, X., DEBRET, M., DENIS, D., COURTY, M.A. & THER, O. 2007. Holocene long- and short-term climate changes off Adélie Land, East Antarctica. *Geochemistry, Geophysics, Geosystems*, **8**, 10.1029/2007GC001718.
- D'ARCY M., SCHILDGEN T.F., STRECKER M.R., WITTMANN H., DUESING W., MEY J., *et al.* 2019. Timing of past glaciation at the Sierra de Aconquija, northwestern Argentina, and throughout the Central Andes. *Quaternary Science Reviews*, **204**, 37–57.
- DARNAULT, R., ROLLAND, Y., BRAUCHER, R., BOURLÈS, D., REVEL, M., SANCHEZ, G. & BOUISSOU, S. 2012. Timing of the last deglaciation revealed by receding glaciers at the Alpine-scale: impact on mountain geomorphology. *Quaternary Science Reviews*, **31**, 127–142.
- DOMACK, E.W., JULL, A.T., ANDERSON, J.B., LINICK, T.W. & WILLIAMS, C.R. 1989. Application of tandem accelerator mass-spectrometer dating to late Pleistocene-Holocene sediments of the East Antarctic continental shelf. *Quaternary Research*, **31**, 277–287.
- DUCLAUX, G., ROLLAND, Y., RUFFET, G., MÉNOT, R.P., GUILLOT, S., PEUCAT, J.J., *et al.* 2008. Superimposed Neoproterozoic and Paleoproterozoic tectonics in the Terre Adélie craton (East Antarctica): evidence from Th-U-Pb ages on monazite and  $^{40}\text{Ar}/^{39}\text{Ar}$  ages. *Precambrian Research*, **167**, 316–338.
- EHLERS, T.A., CHAUDHRI, T., KUMAR, S., FULLER, C.W., WILLET, S.D., KETCHAM, R.A., *et al.* 2005. Computational tools for low-temperature thermochronometer interpretation. *Reviews in Mineralogy and Geochemistry*, **58**, 589–622.
- FERRACCIOLI, F., FINN, C.A., JORDAN, T.A., BELL, R.E., ANDERSON, L.M. & DAMASKE, D. 2011. East Antarctic rifting triggers uplift of the Gamburtsev Mountains. *Nature*, **479**, 388–392.
- FITZGERALD, P.G. 1994. Thermochronologic constraints on post-Paleozoic tectonic evolution of the central Transantarctic Mountains, Antarctica. *Tectonics*, **13**, 818–836.
- GENTHON, C., LARDEUX, P. & KRINNER, G. 2007. The surface accumulation and ablation of a coastal blue-ice area near Cap Prudhomme, Terre Adélie, Antarctica. *Journal of Glaciology*, **53**, 635–645.
- GODARD, G., REYNES, J., BASCOU, J., MÉNOT, R.P. & PALMERI, R. 2017. First rocks sampled in Antarctica (1840): insights into the landing area and the Terre Adélie craton. *Comptes Rendus Geoscience*, **349**(1), 12–21.
- GOLLEDGE, N.R., FOGWILL, C.J., MACKINTOSH, A.N. & BUCKLEY, K.M. 2012. Dynamics of the last glacial maximum Antarctic ice-sheet and its response to ocean forcing. *Proceedings of the National Academy of Sciences of the United States of America*, **109**, 16052–16056.
- HEYMAN, J., STROEVEN, A.P., HARBOR, J.M. & CAFFEE, M.W. 2011. Too young or too old: evaluating cosmogenic exposure dating based on an analysis of compiled boulder exposure ages. *Earth and Planetary Science Letters*, **302**, 71–80.
- ISELL, J.L., HENRY, L.C., GULBRANSON, E.L., LIMARINO, C.O., FRAISER, M.L., KOCH, Z.J., *et al.* 2012. Glacial paradoxes during the Late Paleozoic Ice Age: evaluating the equilibrium line altitude as a control on glaciation. *Gondwana Research*, **22**, 1–19.
- KORSCHINEK, G., BERGMAIER, A., FAESTERMANN, T., GERSTMANN, U.C., KNIE, K., RUGEL, G., *et al.* 2010. A new value for the half-life of  $^{10}\text{Be}$  by heavy-ion elastic recoil detection and liquid scintillation counting. *Nuclear Instruments and Methods in Physics Research Section B: Beam Interactions with Materials and Atoms*, **268**, 187–191.
- LAMARQUE, G., BARRUOL, G., FONTAINE, F.R., BASCOU, J. & MÉNOT, R.P. 2015. Crustal and mantle structure beneath the Terre Adélie craton, East Antarctica: insights from receiver function and seismic anisotropy measurements. *Geophysical Journal International*, **200**, 809–823.
- LAMARQUE, G., BASCOU, J., MÉNOT, R.P., PAQUETTE, J.L., COUZINIÉ, S., ROLLAND, Y. & COTTIN, J.Y. 2018. Ediacaran to lower Cambrian basement in eastern George V Land (Antarctica): evidence from U-Pb dating of gneiss xenoliths and implications for the South Australia-East Antarctica connection. *Lithos*, **318**, 219–229.
- LI, F., MA, C., ZHANG, S., LEI, J., HAO, W., ZHANG, Q. & LI, W. 2020. Evaluation of the glacial isostatic adjustment (GIA) models for Antarctica based on GPS vertical velocities. *Science China Earth Sciences*, **63**, 575–590.
- LIFTON, N. 2016. Implications of two Holocene time dependent geomagnetic models for cosmogenic nuclide production rate scaling. *Earth and Planetary Science Letters*, **433**, 257–268.
- LISKER, F. & OLESCH, M. 2003. Long-term landscape evolution of George V Land as indicated by fission track data. *Terra Antarctica*, **10**, 249–256.
- MACKINTOSH, A., WHITE, D., FINK, D., GORE, D.B., PICKARD, J. & FANNING, P.C. 2007. Exposure ages from mountain dipsticks in Mac. Robertson Land, East Antarctica, indicate little change in ice-sheet thickness since the Last Glacial Maximum. *Geology*, **35**, 551–554.
- MARITATI, A., AITKEN, A.R.A., YOUNG, D.A., ROBERTS, J.L., BLANKENSHIP, D.D. & SIEGERT, M.J. 2016. The tectonic development and erosion of the Knox subglacial sedimentary basin, East Antarctica. *Geophysical Research Letters*, **43**, 10728–10737.
- MONTAÑEZ, I.P., MCELWAIN, J.C., POULSEN, C.J., WHITE, J.D., DiMICHELE, W.A., WILSON, J.P. & HREN, M.T. 2016. Climate,  $p\text{CO}_2$  and terrestrial carbon cycle linkages during late Paleozoic glacial-interglacial cycles. *Nature Geoscience*, **9**, 824–828.
- MORLIGHEM, M., RIGNOT, E., BINDER, T., BLANKENSHIP, D., DREWS, R., EAGLES, G., *et al.* 2019. Deep glacial troughs and stabilizing ridges unveiled beneath the margins of the Antarctic ice sheet. *Nature Geoscience*, **13**, 132–137.
- NAUMENKO-DÉZES, M.O., ROLLAND, Y., LAMARQUE, G., DUCLAUX, G., GALLET, S., BASCOU, J. & MÉNOT, R.P. 2020. Petrochronology of the Terre Adélie craton (East Antarctica) evidences a long-lasting Proterozoic (1.7–1.5 Ga) tectono-metamorphic evolution - insights for the connections with the Gawler craton and Laurentia. *Gondwana Research*, **81**, 21–57.
- PAXMAN, G.J., JAMIESON, S.S., HOCHMUTH, K., GOHL, K., BENTLEY, M.J., LEITCHENKOV, G. & FERRACCIOLI, F. 2019. Reconstructions of Antarctic topography since the Eocene-Oligocene boundary. *Palaeogeography, Palaeoclimatology, Palaeoecology*, **535**, 109346.
- PEUCAT, J.J., CAPDEVILA, R., FANNING, C.M., MÉNOT, R.P., PÉCORA, L. & TESTUT, L. 2002. 1.60 Ga felsic volcanic blocks in the moraines of the Terre Adélie craton, Antarctica: comparisons with the Gawler Range Volcanics, South Australia. *Australian Journal of Earth Sciences*, **49**, 831–845.
- PUTKONEN, J. & SWANSON, T. 2003. Accuracy of cosmogenic ages for moraines. *Quaternary Research*, **59**, 255–261.

- QIE, W., ALGEO, T.J., LUO, G. & HERRMANN, A. 2019. Global events of the Late Paleozoic (Early Devonian to Middle Permian): a review. *Palaeogeography, Palaeoclimatology, Palaeoecology*, **531**, 109259.
- RIGNOT, E., MOUGINOT, J. & SCHEUCHL, B. 2011. Ice flow of the Antarctic ice sheet. *Science*, **333**, 1427–1430.
- RITZ, C., EDWARDS, T.L., DURAND, G., PAYNE, A.J., PEYAUD, V. & HINDMARSH, R.C. 2015. Potential sea-level rise from Antarctic ice-sheet instability constrained by observations. *Nature*, **528**, 115–118.
- ROLLAND, Y., BERNET, M., VAN DER BEEK, P., GAUTHERON, C., DUCLAUX, G., BASCOU, J., *et al.* 2019. Late Paleozoic Ice Age glaciers shaped East Antarctica landscape. *Earth and Planetary Science Letters*, **506**, 123–133.
- RYGEL, M.C., FIELDING, C.R., FRANK, T.D. & BIRGENHEIER, L.P. 2008. The magnitude of Late Palaeozoic glacioeustatic fluctuations: a synthesis. *Journal of Sedimentary Research*, **78**, 500–511.
- STEIG, E.J., MORSE, D.L., WADDINGTON, E.D., STUIVER, M., GROOTES, P.M., MAYEWSKI, P.A., *et al.* 2000. Wisconsinan and Holocene climate history from an ice core at Taylor Dome, western Ross Embayment, Antarctica. *Geografiska Annaler*, **82**, 213–235.
- THOMSON, S.N., REINERS, P.W., HEMMING, S.R. & GEHRELS, G.E. 2013. The contribution of glacial erosion to shaping the hidden landscape of East Antarctica. *Nature Geoscience*, **6**, 203–207.
- TISON, J.L., PETIT, J.R., BARNOLA, J.M. & MAHANEY, W.C. 1993. Debris entrainment at the icebedrock interface in sub-freezing temperature conditions (Terre Adelie, Antarctica). *Journal of Glaciology*, **39**, 303–315.
- TORSVIK, T.H., MÜLLER, R.D., VAN DER VOO, R., STEINBERGER, B. & GAINA, C. 2008. Global plate motion frames: toward a unified model. *Review of Geophysics*, **46**, 1–44.
- VERLEYEN, E., HODGSON, D.A., MILNE, G.A., SABBE, K. & VYVERMAN, W. 2005. Relative sea-level history from the Lambert Glacier region, East Antarctica, and its relation to deglaciation and Holocene glacier readvance. *Quaternary Research*, **63**, 45–52.
- VERLEYEN, E., HODGSON, D.A., SABBE, K., CREMER, H., EMSLIE, S.D., GIBSON, J., *et al.* 2011. Postglacial regional climate variability along the East Antarctic coastal margin evidence from shallow marine and coastal terrestrial records. *Earth-Science Reviews*, **104**, 199–212.
- ŽEBRE, M., SARIKAYA, M.A., STEPIŠNIK, U., YILDIRIM, C. & ÇINER, A. 2019. First <sup>36</sup>Cl cosmogenic moraine geochronology of the Dinaric mountain karst: Velež and Crvanj Mountains of Bosnia and Herzegovina. *Quaternary Science Reviews*, **208**, 54–75.
- ZWARTZ, D., BIRD, M., STONE, J. & LAMBECK, K. 1998. Holocene sea-level change and ice-sheet history in the Vestfold Hills, East Antarctica. *Earth and Planetary Science Letters*, **155**, 131–145.